Article

Not peer-reviewed version

Genome-Wide Characterization of the ANN Gene Family in *Corydalis saxicola* and the Role of CsANN1 in Dehydrocavidine Biosynthesis

Han Liu , Jing Wang , Zhaodi Wen , Mei Qin , Ying Lu , Lirong Huang , Xialian Ou , Liang Kang , Cui Li , Ming Lei * , Zhanjiang Zhang *

Posted Date: 21 May 2025

doi: 10.20944/preprints202505.1673.v1

Keywords: annexin; *Corydalis saxicola*; calcium; benzylisoquinoline alkaloid

 doi:10.20944/preprints202505.1673.v1

Article

Genome-Wide Characterization of the *ANN* Gene Family in *Corydalis saxicola* and the Role of CsANN1 in Dehydrocavidine Biosynthesis

Han Liu [1,2,3], Jing Wang [1,2,3], Zhaodi Wen [1,2,4], Mei Qin [1,2,3], Ying Lu [1,2,4], Lirong Huang [1,2,3], Xialian Ou [1,2,3], Liang Kang [1,2,4] Cui Li [1,2,3], Ming Lei [1,2,3,*] and Zhanjiang Zhang [1,2,3,5,*]

[1] Guangxi Key Laboratory of Medicinal Resources Protection and Genetic Improvement, Guangxi Botanical Garden of Medicinal Plants, Nanning 530023, China
[2] National Center for Traditional Chinese Medicine (TCM) Inheritance and Innovation, Guangxi Botanical Garden of Medicinal Plants, Nanning 530023, China
[3] Guangxi Engineering Research Center of TCM Resource Intelligent Creation, Guangxi Botanical Garden of Medicinal Plants, Nanning 530023, China
[4] School of Pharmacy, Guangxi Medical University, Nanning 530021, China
[5] Guangxi Key Laboratory for High-Quality Formation and Utilization of Dao-di Herbs, Guangxi Botanical Garden of Medicinal Plants, Nanning 530023, China
* Correspondence: leiming@gxyyzwy.com (M.L.); zzj1811@163.com (Z.Z.)

Abstract: Annexins (ANNs), which are calcium (Ca^{2+})-dependent and phospholipid-binding protein families, are implicated in the regulation of plant growth and development as well as protection from various stresses. However, little is known about ANNs in *Corydalis Saxicola*, an endangered benzylisoquinoline alkaloid (BIA)-riched herbaceous plant widely used in traditional Chinese medicine and endemic to the calciphilic karst region in China. Here, nine *CsANN* genes were identified from *C. saxicola*, and they were divided into three subfamilies based on the phylogenetic analysis. The CsANNs clustered into the same clade, sharing similar gene structures and conserved motifs. The nine *CsANN* genes were located on five chromosomes, and their expansions were mainly attributed to tandem duplication and segmental duplication. The *CsANN* transcripts showed variable organ-specific and Ca^{2+}-responsive expression patterns. Further transient overexpression assays showed that CsANN1 could positively regulate the accumulation of BIA compounds in *C. saxicola* leaves, probably through directly interacting with key BIA-biosynthesis-pathway enzymes or by interacting with BIA-biosynthesis-regulating factors, such as MYBs. This study sheds light on profiles and functions of the *CsANN* gene family and paves the way for unraveling the molecular mechanism of BIA accumulation regulated by Ca^{2+} through CsANNs.

Keywords: annexin; *Corydalis saxicola*; calcium; benzylisoquinoline alkaloid

1. Introduction

Corydalis saxicola Bunting, which belongs to the genus *Corydalis* within the Papaveraceae family, is an endangered herbaceous plant widely used in traditional Chinese medicine due to its various pharmacological activities, including anti-cancer, anti-inflammatory, antibacterial, antioxidant, and analgesic properties [1–3]. These pharmacological activities of Yanhuanglian (the Chinese name of *C. saxicola*) are primarily attributed to the presence of benzylisoquinoline alkaloid (BIA) compounds, with dehydrocavidine (DHCA) identified as one of the key active ingredients [4,5]. As a species endemic to the karst region in China, *C. saxicola* lives exclusively in or around rock crevices and demonstrates good adaptability to the arid, infertile, and calcium-rich soils, which are the typical karst environments [6]. However, both its narrow, stringent karst-adapted habitat and the imbalance of large market demand make it endangered [6–8]. Therefore, understanding the adaptation

 doi:10.20944/preprints202505.1673.v1

mechanism of *C. saxicola* in calcium-rich karst habitats, as well as the regulatory molecular mechanism of the key active BIAs, such as DHCA, in *C. saxicola*, are considered as two of the most efficient and promising approaches for the conservation and utilization of this endangered medicinal plant.

Annexins (ANNs) are evolutionarily conserved, water-soluble proteins [9]. The plant ANNs, which can bind to or insert into cell membranes and regulate the homeostasis of free Ca^{2+} in the cytoplasm, are the members of voltage-gated Ca^{2+} channels [10]. In addition, it has peroxidase as well as ATPase/GTPase activities, which give ANNs functional specificity [11,12]. The core structures of plant ANNs are characterized by a N-terminal region and a C-terminal region [12]. The short N-terminal region comprises approximately a dozen amino acids and is commonly as the site for secondary modifications, including phosphorylation, nitrosylation, S-glutathionylation, and N-myristoylation, which are regulated by various signaling pathways [9,13,14]. Biochemical experiments have demonstrated that the N-terminal domain modulates different ANN properties through its allosteric mechanism [9,15]. The C-terminal region of plant ANNs contains four conservative ANN repeats, each repeat containing about 70 amino acid residues and then folding into five α helices [16]. Specifically, both of the repeats I and IV include a motif of GXGT-(38 variable amino acid residues)-D/E, which was considered as a Ca^{2+} binding site [17]. However, compared to that in the repeat I, this motif is less conserved in the repeat IV [18]. Recently, the ANN families have been identified in many plant species, including *Carica papaya*, *Glycine max*, *Oryza sativa*, *Raphanus sativus*, *Vitis vinifera*, *Zea mays*, and so on [19–23]. These ANNs are ubiquitously distributed across various plant tissues, including embryos, seedlings, roots and tubers, stems, hypocotyls and cotyledons, leaves, inflorescences, fruits, vascular systems, and phloem sap [24–28], demonstrating their wide involvements in regulating of biochemical and cellular processes, plant growth and development, and response to biotic and abiotic stresses [9–11,14].

Plants in karst areas generally have the tolerance to drought and calciphilic characteristics [29,30]. Our previous studies found that the cultivated *C. saxicola* plants had the ability to endure the treatment of high concentrations of exogenous $CaCl_2$ solutions for nearly a month at least, and the contents of DHCA in the roots of *C. saxicola* were significantly enhanced after the treatments. Nevertheless, how extracellular Ca^{2+} signaling was recognized and converted into intracellular ones to regulate the biosynthesis of DHCA in *C. saxicola* is largely unknown. As plant ANNs are members of voltage-gated Ca^{2+} channels and are involved in Ca^{2+} uptake and transport, we speculated that ANNs in *C. saxicola* (CsANNs) might be one of the key executors during this process.

In this study, a global survey of the nine *ANN* genes in the *C. saxicola* genome was conducted. The physicochemical properties, conserved motifs, gene structures, and cis-elements in the promoter regions of *CsANN*s were identified. In addition, the homologous *ANN* genes from different species were determined based on a collinearity analysis. Furthermore, the expression profiles of all nine *CsANN*s in different tissues and under $CaCl_2$ treatments were analyzed. The transient overexpression assays demonstrated that CsANN1 could induce the accumulation of DHCA in the leaves of *C. saxicola*. In summary, the present study might provide substantial useful information for the understanding of CsANNs as the key effectors during Ca^{2+} uptake and transport, and the role played in the biosynthesis of DHCA in *C. saxicola*.

2. Results

2.1. Identification and Physicochemical Analysis of CsANNs

A total of nine candidate *ANN*s were identified in the *C. saxicola* genome. All these CsANNs contained conserved ANN domains, indicating that these peptides were putative ANNs. Subsequently, all nine *CsANN* genes were successfully cloned by PCR and verified by Sanger sequencing. Consequently, these *CsANN*s were named as *CsANN1-9* according to their chromosomal localization (Table S1).

 doi:10.20944/preprints202505.1673.v1

Physicochemical property analysis results showed that the CsANN proteins contained 316 to 341 amino acids, with molecular weights (MWs) ranging from 35.48 kDa to 38.67 kDa (Table S1). The hydrophilicities of the nine CsANN proteins were all below 0, indicating their hydrophilic nature. The isoelectric points (pIs) of CsANN1, 5, 6, 7, and 9 were all below 7, indicating that they were acidic hydrophilic proteins; the others were basic hydrophilic proteins. The protein instability indices of CsANN1, 3, 4, 5, and 7 were below 40, and these are stable proteins; the others were unstable proteins. The results of subcellular localization of CsANNs predicted by different software were variable, but most of them localized in the cytosol (Figure 1A).

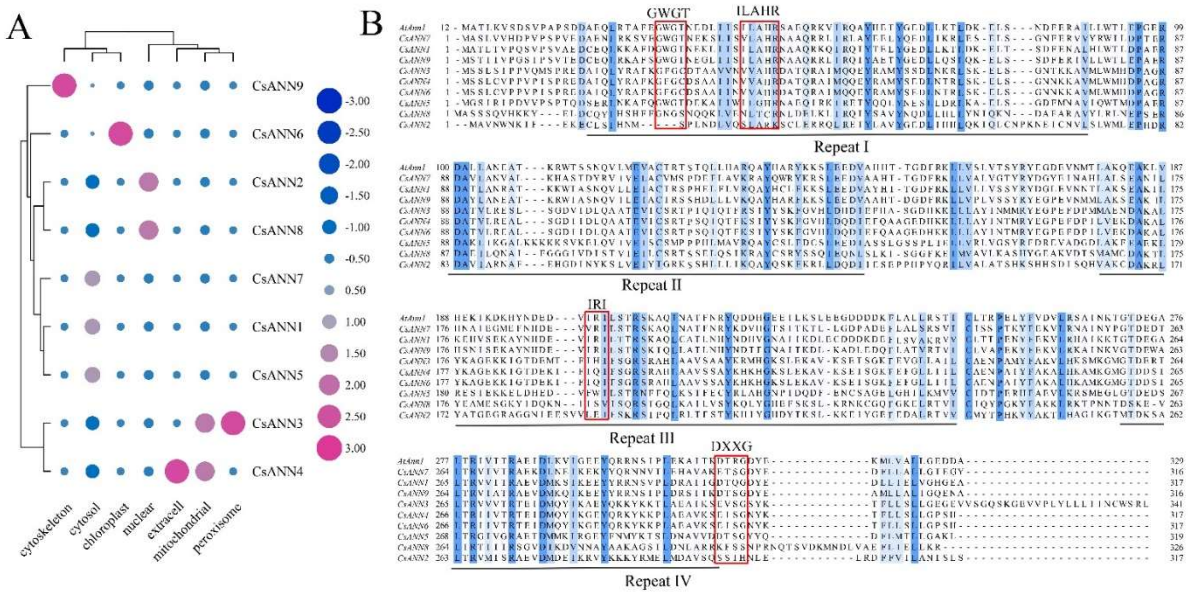

Figure 1. The heatmap of the subcellular localizations of CsANNs (A) and multiple sequence alignments of deduced amino acid sequences of ANN proteins from *C. saxicola* and *Arabidopsis thaliana* (B).

2.2. Sequences Alignment and Phylogenetic Analysis of ANNs

The amino acid sequence alignment results indicated that CsANN proteins contained four conserved ANN repeats, each of which consisted of approximately 70 amino acids and was similar to that of AtANN1 (Figure 1B). Particularly, the specific Ca^{2+}-binding sites (G/KXGT-38-D/E), which could functionally bind to phospholipid membranes, were characterized in the repeat I of CsANN1, 5, 7, and 9 (Figure 1B). In addition, a conserved peroxidase residue (ILAHR) was identified in CsANN1, 5, and 9, indicating that they were likely to have peroxidase activity. Furthermore, the IRI site, which could bind to F-actin, existed in the repeat III of CsANN1 and 9, and the DXXG site, which could bind to GTP, was found in the repeat IV of CsANN1, 5, and 9 (Figure 1B).

To elucidate the evolutionary patterns and potential functions of CsANNs, we used the neighbor-joining (NJ) method to construct a phylogenetic tree based on 111 ANN proteins from nine species. As shown in Figure 2, all the ANNs could be divided into four subfamilies according to the phylogenetic tree analysis. CsANNs were distributed among all subfamilies except subfamily III, and their distribution pattern was similar with other ANNs except two ones of *C. yanhusuo* (CyANN16 and CyANN24) (Figure 2). Among all nine CsANNs, CsANN1, 7, and 9 were classified within subfamily I, CsANN2, 3, 4, 6, and 8 were assigned to subfamily IV, and only CsANN5 was categorized under subfamily II (Figure 2). Typically, CsANNs were initially grouped with CtANNs and CyANNs, followed by PtANNs and AtANNs within each clade, suggesting a closer evolutionary relationship among CtANNs, CyANNs, and CsANNs (Figure 2). Conversely, the evolutionary relationships among ANN proteins from *C. saxicola*, *Hordeum vulgare*, and *O. sativa* were found to be the farthest (Figure 2). These findings indicated that CsANNs were more closely related to those of

 doi:10.20944/preprints202505.1673.v1

dicotyledons than those of monocotyledons, which was consistent with previous studies [18,19,21,22].

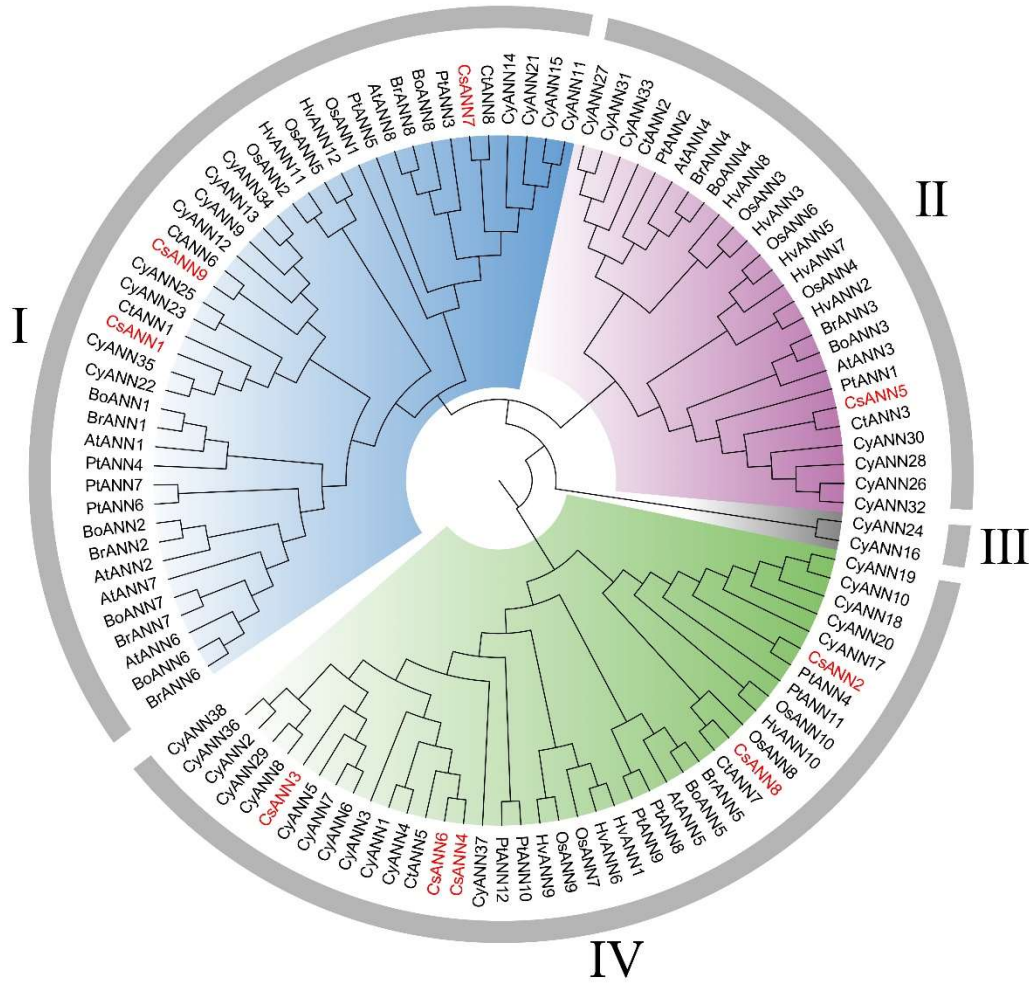

Figure 2. The phylogenetic tree of the ANN proteins. At: Arabidopsis thaliana; Bo: Brassica oleracea; Br: Brassica rapa; Ct: Corydalis tomentella; Cy: Corydalis yanhusuo; Hv: Hordeum vulgare; Os: Oryza sativa; Pt: Populus tremula x Populus.

2.3. Conserved Motifs and Gene Structure of CsANNs

The gene structure characteristics of *CsANN*s, and the conserved motifs and domain compositions of CsANN proteins were analyzed and shown according to their phylogenetic relationships (Figure 3A). Four or five motifs were characterized in CsANNs, and motif 1~4 were commonly identified in all CsANNs (Figure 3B). CsANN2 and CsANN8, two members of Subfamily IV, lack motif 5, potentially causing functional loss (Figure 3B). Additionally, all CsANNs have four ANN domains except CsANN2 and CsANN8, which lack one and two ANN domains, respectively (Figure 3C). The exon-intron structural analysis showed that the number of exons within the *CsANN* genes varied between 4 and 7 (Figure 3D). Notably, *CsANN3* contained 7 exons, and *CsANN8* contained 4 exons (Figure 3D). It should be mentioned that among all *CsANN*s, *CsANN1* possesses the longest introns (Figure 3D). Furthermore, *CsANN*s within the same evolutionary branches, specifically subfamily I (*CsANN1* and *CsANN9*) and subfamily IV (*CsANN4* and *CsANN6*), exhibited similar intron/exon patterns (Figure 3D).

 doi:10.20944/preprints202505.1673.v1

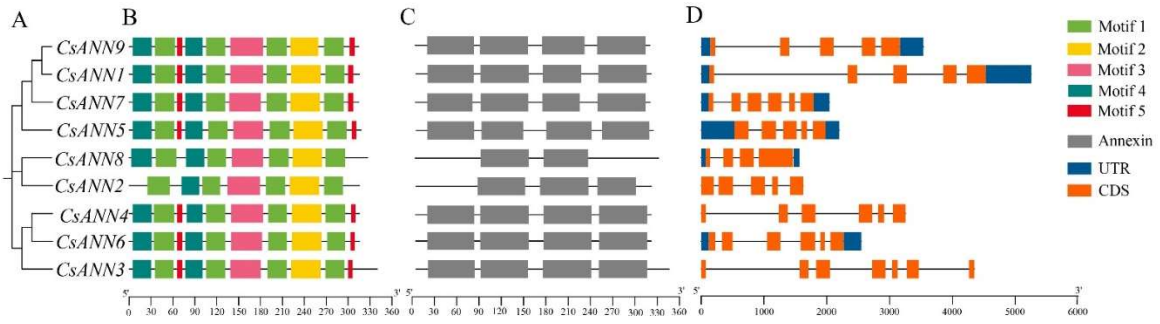

Figure 3. The phylogenetic relationship, conserved motifs, ANN domains of CsANN proteins, and the intron and exon compositions of *CsANN* genes.

2.4. Chromosomal Location and Collinearity Analysis of CsANNs

A chromosomal location map was constructed to investigate the genetic divergence and duplication within the *CsANN*s. Nine *CsANN* genes were identified and localized on five chromosomes. The distribution of *CsANN*s on each chromosome appeared relatively independent and irregular. Among these chromosomes, chromosome 8 contained the highest number of *CsANN*s, with three identified, followed by chromosomes 6 and 7, each with two *CsANN*s. Chromosomes 1 and 2 each contained a single *CsANN* gene (Figure 4A).

To further elucidate the expansion mechanism of the *CsANN* gene family, we performed collinearity and duplication analyses using TBtools [31]. Intraspecific collinearity analysis revealed the presence of one pair of collinear genes in *C. saxicola* (*CsANN1*-*CsANN9*), both were attributed to segmental duplication, and *CsANN3*, *4*, *5*, and *6* came from tandem repetition (Figure 4B). These indicate that segmental duplication events and tandem repetition events were pivotal for the expansion of *CsANN*s during evolution.

To explore the underlying evolutionary mechanisms of *CsANN*s, we selected five representative angiosperm species, including *A. thaliana*, *C. tomentella*, *H. vulgare*, *O. sativa*, and *P. tremula*, to construct collinearity analysis maps with *C. saxicola*. The analysis revealed that the *CsANN*s exhibited the highest syntenic relationships with ANNs in *P. tremula* (10), followed by *C. tomentella* (8), *A. thaliana* (5), *H. vulgare* (4), and *O. sativa* (3) (Figure 5). Those results indicated that the *ANN* genes from *C. saxicola*, *P. tremula* and *C. tomentella* had a close relationship. In addition, a greater number of *ANN* homologous genes were identified in dicotyledons than those in monocotyledons (Figure 5).

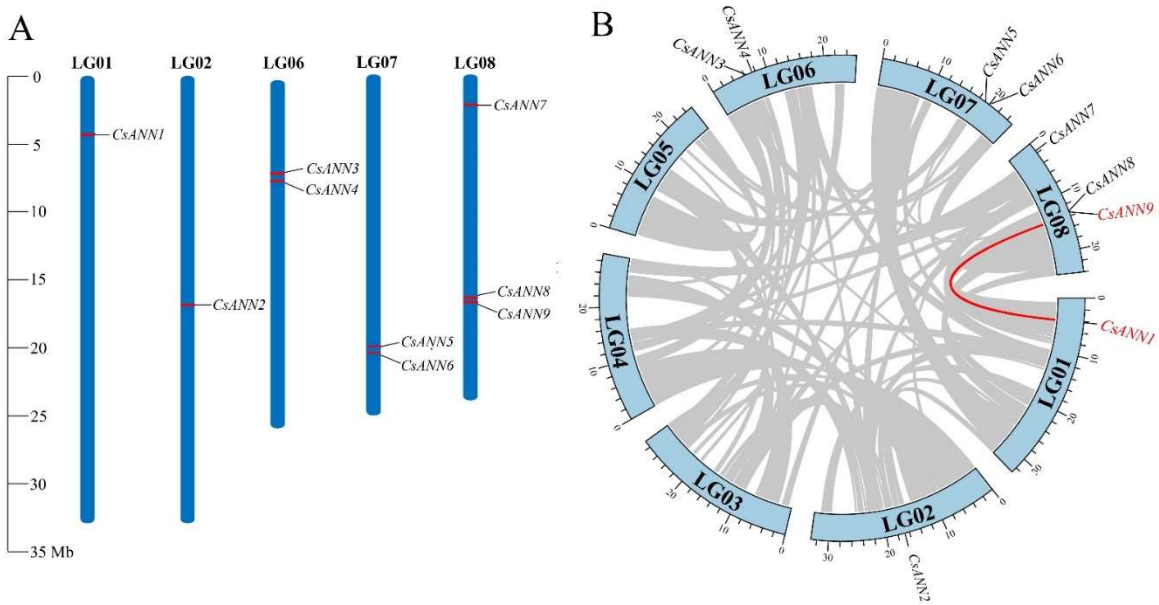

 doi:10.20944/preprints202505.1673.v1

Figure 4. Location distribution of *CsANN* genes on *C. saxicola* chromosomes (A) and synteny analysis of *CsANN* genes (B).

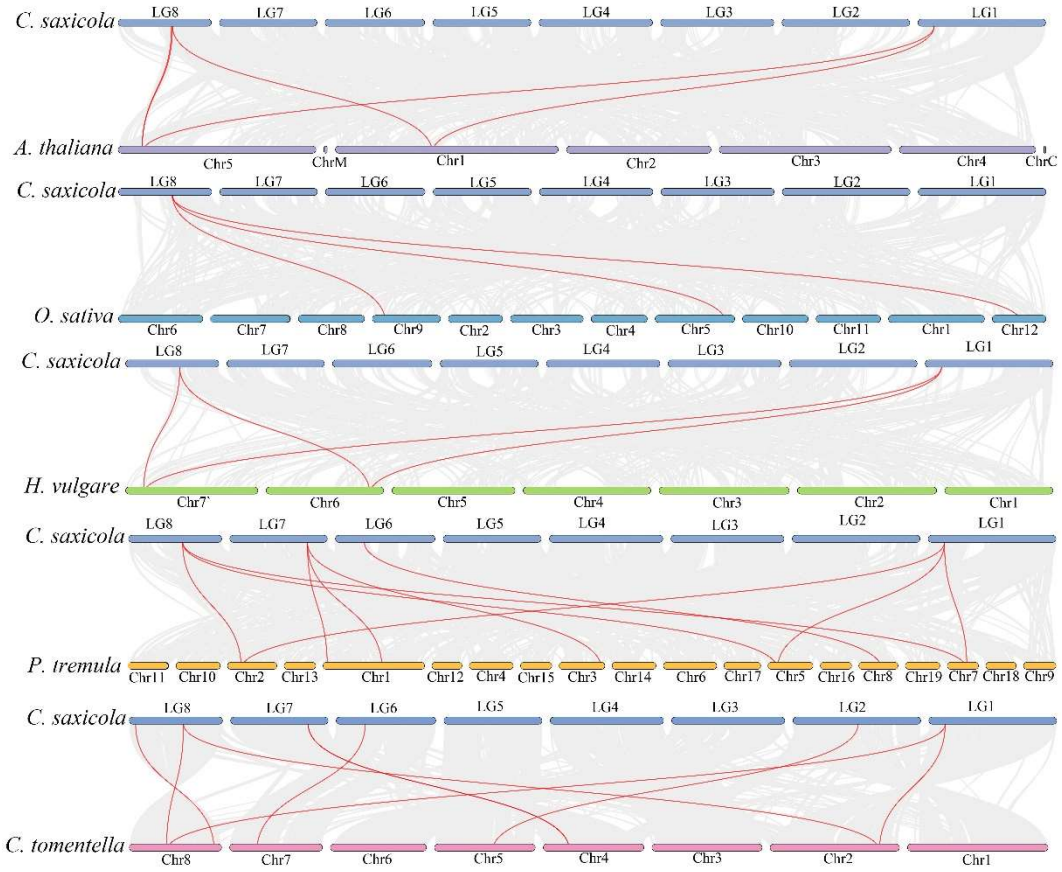

Figure 5. Extra-genomic collinearity related to *CsANN* genes in *A. thaliana*, *C. saxicola*, *C. tomentella*, *H. vulgare*, *O. sativa*, and *P. tremula*.

2.5. Analysis of Cis-Acting Elements in CsANN Promoters

To further investigate the response of *CsANN*s to stresses, we used PlantCARE to extract cis-acting elements involved in plant hormone regulation and abiotic stress response from 2.0 kb 5′ upstream regions of *CsANN*s [32]. As shown in Figure 6, five main categories of cis-acting elements were predicted, including oxidative stress- (ARE-motif), cold stress- (LTR-motif), drought stress- (MBS-motif), light- (Box 4, GATA-motif, G-Box, G-Box, GT1-motif, TCT-motif), and plant hormone- (abscisic acid response element, ABRE; methyl jasmonate response element, CGTCA-motif, TGACG-motif; gibberellin response element, GARE-motif, P-box; auxin response element, TGA-element) responsive elements. All *CsANN*s, except *CsANN4*, contain light-responsive elements. Cis-acting elements associated with hormonal responses were also found in all *CsANN* promoters, except *CsANN1*. *CsANN1*, *7*, and *4* contain elements related to drought response. *CsANN4*, *7*, and *9* contain elements related to low temperature response. Only *CsANN7* promoters have been identified as a role involved in the antioxidant response. In addition, the GTGGC-motif was only present in *CsANN9*. The TGACG-motif, which was suggested to be involved in the methyl jasmonate response, appeared only in *CsANN3*. The P-box, one of the gibberellin response elements, was present in the promoters of *CsANN4* and *CsANN9*. The GARE-motif was present in the promoters of *CsANN8* and *CsANN9*. It should be mentioned that all *CsANN*s had MYB transcription factor binding sites (Table S2). All the observations indicated that *CsANN* genes might be involved in environmental stress response and hormone regulation, and play essential roles in physiological and developmental processes of *C. saxicola*.

 doi:10.20944/preprints202505.1673.v1

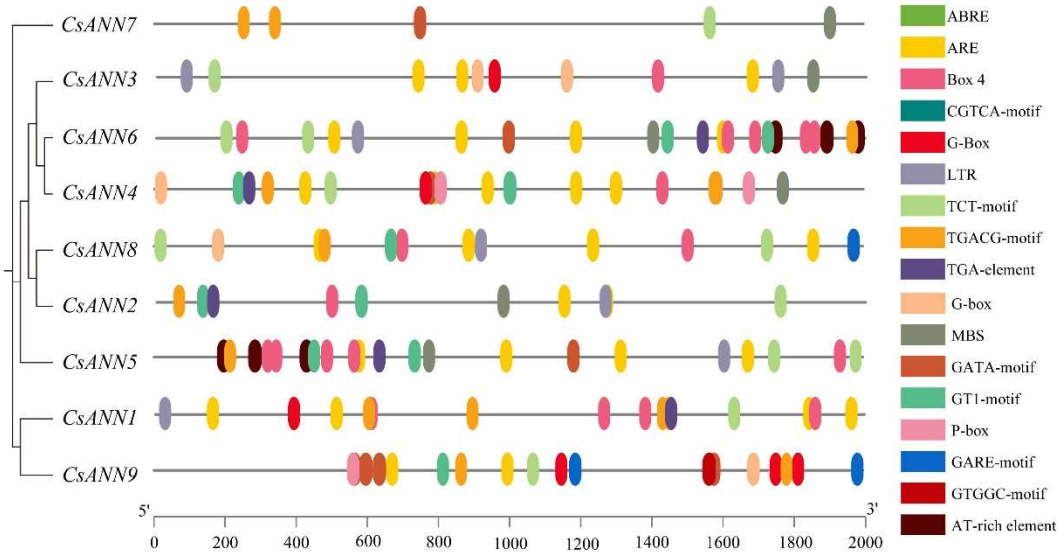

Figure 6. The distribution of cis-acting elements in promoters of *CsANN*s.

2.6. Tissue-Specific Expression Profile of CsANNs

The quantitative real time PCR (qRT-PCR) analysis results indicated that the expression patterns of the *CsANN*s were variable in different tissues of *C. saxicola*. As shown in Figure 7, the *CsANN2*, *CsANN3*, *CsANN4*, and *CsANN8* were greatly expressed in flowers, suggesting their potentially significant biological role in flowering phase transition or flowering organ development. *CsANN5* and *CsANN6* were particularly highly expressed in the stems, indicating that they might be involved in the development of the stems of *C. saxicola*. We also observed that some *CsANN* genes (*CsANN2*, *CsANN7*, and *CsANN8*) displayed high expression in fruit pods of *C. saxicola*. Interestingly, *CsANN1*, *CsANN3*, *CsANN4*, and *CsANN9* showed relatively high accumulation in the roots of *C. saxicola*.

 doi:10.20944/preprints202505.1673.v1

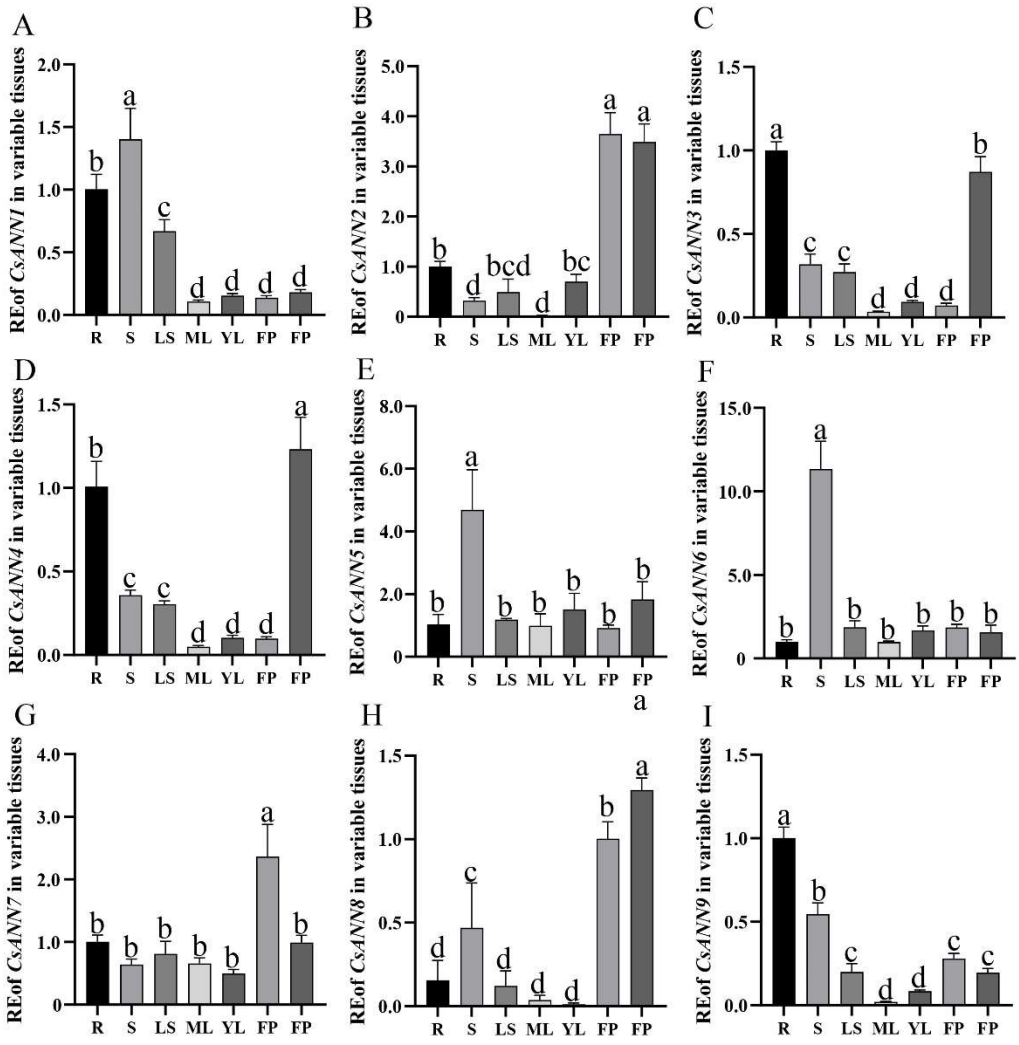

Figure 7. Relative expression (RE) levels of *CsANN*s in different tissues of *C. saxicola.* R: roots, S: ems, LS: lateral stems, ML: mature leaves, YL: young leaves, FP: fruit pods, F: flowers.

2.7. The Effects of Exogenous $CaCl_2$ Treatments on C. saxicola Seedlings

In order to investigate whether Ca^{2+} influences the growth and development of *C. saxicola*, different concentrations of exogenous $CaCl_2$ were used to treat one-month-old *C. saxicola* seedlings. As shown in Figure 8A-C, the calcium content, proline content, and soluble sugar content of *C. saxicola* leaves were significantly increased with the elevation of exogenous $CaCl_2$ concentrations ($P < 0.05$). In addition, significant differences in the DHCA content in the stems, leaves, and roots of *C. saxicola* after treatments were also observed ($P < 0.05$), and the content of DHCA in roots was much higher than that in stems and leaves (Figure 8D-F). Interestingly, the high concentration of exogenous $CaCl_2$ significantly induced the accumulation of DHCA in the roots of *C. saxicola* (Figure 8F).

We then analyzed the FPKM values of *CsANN*s based on the transcriptomic data. It was found that, except for *CsANN2* and *CsANN8*, the FPKM values of other *CsANN*s showed significant changes with the increase of $CaCl_2$ concentration ($P < 0.05$) (Figure 8G-O). Especially, the FPKM values of *CsANN1* and *CsANN9* are positively correlated with calcium concentration (Figure 8G, O).

 doi:10.20944/preprints202505.1673.v1

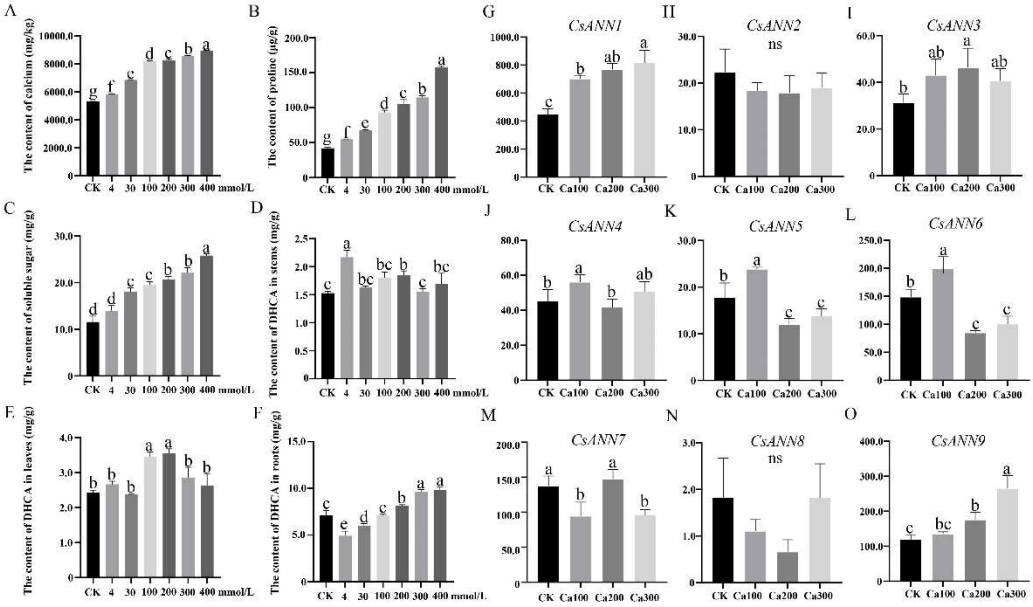

Figure 8. The effects of exogenous $CaCl_2$ treatments on *C. saxicola* seedlings. A-C: The calcium content, proline content, and soluble sugar content in mature leaves of *C. saxicola* under the treatments of different $CaCl_2$ concentrations. D-F: The DHCA content in stems, mature leaves, and roots of *C. saxicola* under the treatments of different $CaCl_2$ concentrations. G-O: Relative expression levels of *CsANN*s treated with different concentrations of $CaCl_2$.

2.8. CsANNs Correlated with DHCA Biosynthesis

According to the predicted biosynthetic pathway of DHCA, C-methyltransferases (CMTs), O-methyltransferases (OMTs), and berberine bridge enzyme-likes (BBELs) were involved in the transition of cheilanthifoline into DHCA [33]. In order to elucidate the relationship between CsANNs and the above key enzymes involved in the DHCA biosynthesis, we conducted a correlation analysis among *CsCMT*s, *CsOMT*s, *CsBBEL*s, and *CsANN*s. An interaction network that comprised 34 nodes and 66 relational pairs with high correlations ($R \geq 0.8$ and $P \leq 0.05$ or $R \leq -0.8$ and $P \leq 0.05$) was identified. Among them, four major sub-networks (*CsANN1*, *CsANN5*, *CsANN6*, *CsANN9*), which collectively included 48 relational pairs and 25 nodes, were summarized (Figure S2). For *CsANN1*, the connectivity number is 9, and it shows significant correlation with the expression of 3 *CsOMT*s and 6 *CsBBEL*s. Similarly, the connectivity number for *CsANN9* is 11, which is significantly correlated with the expression of 5 *CsOMT*s and 6 *CsBBELs* (Figure S2).

As is mentioned above, the transcripts of both *CsANN1* and *CsANN9* were not only relatively high in the roots of *C. saxicola*, but also positively correlated with the content of DHCA in the roots of *C. saxicola* treated by exogenous $CaCl_2$ solutions. Furthermore, the expression of *CsANN1* and *CsANN9* had high correlations with the expression of DHCA-biosynthetic-related genes (Figure S2). These indicated that CsANN1 and CsANN9 might play positive roles in the biosynthesis of DHCA.

To confirm this speculation, transient overexpression assays of *CsANN1* and *CsANN9* were conducted in *C. saxicola* leaves, respectively (Figure 9A). The transcript levels of *CsANN1* and *CsANN9* in *C. saxicola* leaves infiltrated with *CsANN1*-pCAMBIA1301 and *CsANN9*-pCAMBIA1301 increased significantly compared to the empty vector, respectively (Figure 9B, Figure S3A). Furthermore, the contents of Cheilanthifoline and DHCA in *C. saxicola* leaves infiltrated with *CsANN1*-pCAMBIA1301 were also significantly increased compared to the empty vector (Figure 9C, D). However, compared to the empty vector, the contents of Cheilanthifoline and DHCA in *C. saxicola* leaves infiltrated with *CsANN9*-pCAMBIA1301 did not show significant difference (Figure S3B, C). These results suggested that CsANN1 but not CsANN9 might play a positive role in the biosynthesis of DHCA.

 doi:10.20944/preprints202505.1673.v1

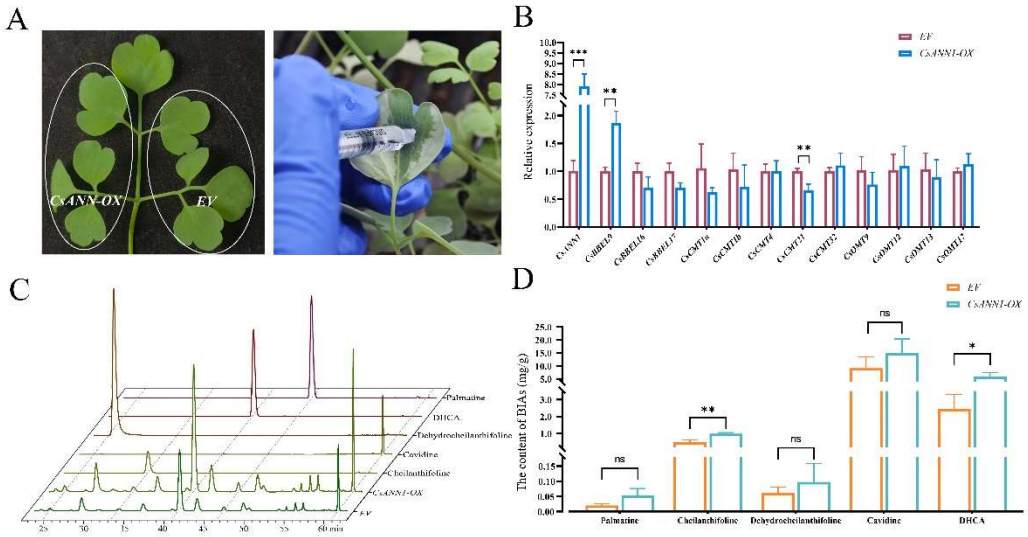

Figure 9. The transient overexpression and functional analysis of *CsANN1*. (A) The schematic diagram of infiltration of *C. saxicola* leaves with *CsANN*-pCAMBIA1301 or EV. (B) Expression profiles of *CsANN1* and other genes in *C. saxicola* leaves infiltrated with *CsANN1*-pCAMBIA1301 or EV. (C) Changes in BIA contents in *C. saxicola* leaves infiltrated with *CsANN1*-pCAMBIA1301 or EV. (D) Statistic analysis of BIA contents in *C. saxicola* leaves infiltrated with *CsANN1*-pCAMBIA1301 or EV.

2.9. Yeast Two Hybrid Assay and Protein Interaction Networks of the CsANNs

Numerous proteins could form dimers, polymers or more complicated complexes to execute biological processes *in vivo* [34,35]. In order to explore whether CsANNs could form homodimers or heterodimers, yeast two-hybrid assays were conducted. As shown in Figure 10A, similar to the negative control pBD, the yeast cells carrying the tested vectors could not grow on the selective solid medium lacking Tyrosine (Trp) but containing 5-Bromo-4-chloro-3-indoxyl-α-D-galactopyranoside (X-α-gal) and Aureobasidin A (AbA), indicating that all CsANNs had no auto-activation activities in Y2HGold cells (Figure 10A). Further assays indicated that either the yeast cells containing the pair of cotransformed indicated plasmids could grow on the selective medium containing X-α-gal and AbA, indicating that none of these CsANNs could form homodimers or heterodimers in yeast cells (Figure 10B).

We then utilized the STRING database and TBtools to further reveal the interactions between CsANNs and other proteins. The results showed that the interaction patterns of CsANN1 with proteins closely resemble those of AtANN1 (Figure 10C). Proteins interacting with AtANN1 include the DEAD-box ATP-dependent RNA helicase (AtRH11, 37, 52) belongs to the DDX3/DED1 subfamily of DEAD box helicase family; probable cyclic nucleotide-gated ion channel (AtCNGC1, 6) belongs to the cyclic nucleotide-gated cation channel; the tetraspanin-8 (AtTET8) belongs to the tetraspanin family; the hyperosmolarity-gated non-selective cation channel (AtOSCA1) belongs to the CSC1 family, among others. Similarly, the interaction patterns of CsANN9 with proteins are similarities to those of AtANN2. AtANN2 is predicted to interact with AtTET8; RGG repeats nuclear RNA binding protein C (AtRGGC); RGG repeats nuclear RNA binding protein B (AtRGGB) belongs to the RGGA protein family; UDP-glucose 6-dehydrogenase 4 (AtUGD4) belongs to the UDP-glucose/GDP-mannose dehydrogenase family, and other proteins. Furthermore, the interaction network of CsANNs suggested potential interactions with proteins such as Glucose-6-phosphate isomerase (GPI); GDP-mannose transporter GONST1 (GDP-Man); ATP dependent RNA helicase DDX3X (DDX3X), among others (Figure 10C). These results indicated that CsANN proteins might be involved in various physiological functions, including transcriptional regulation, RNA stability,

 doi:10.20944/preprints202505.1673.v1

signal transduction, mRNA transport, Golgi secretion, maintenance of cellular osmotic balance, synthesis of cell wall precursors, as well as regulation of calcium channels.

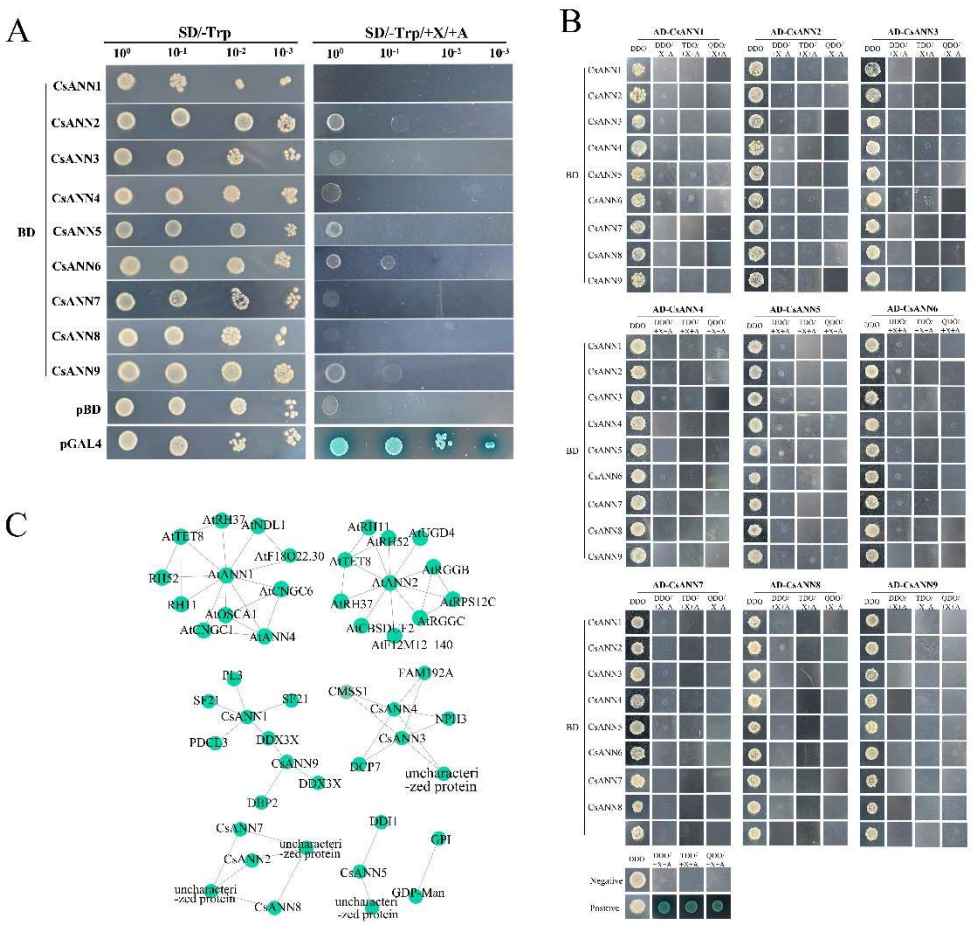

Figure 10. Yeast two hybrid assay and protein interaction networks of the CsANNs. A: Transactivation assay. SD/-Trp: SD medium without Trp, SD/-Trp/+X/+A: SD medium without Trp supplemented with X-α-gal at a concentration of 40 ng/mL, AbA at a concentration of 100 ng/mL. B: Yeast two hybrid assay. DDO: SD medium without Trp and Leu; TDO: SD medium without Trp, Leu, and His; QDO: SD medium without Trp, Leu, His and Ade. C: The protein interaction networks of the CsANNs.

3. Discussion

3.1. The Structure of CsANNs Were Conserved

The ANNs had been identified and functionally analyzed in a variety of plant species, including model plants and crops, but the informations about ANN gene families in medicinal plants were scarce [19,21–23,36,37]. In this study, nine *CsANN* genes were identified based on the genome and transcriptome data of *C. saxicola*, an endangered herbaceous plant that exclusively lived in Chinese karst landforms and was widely used in traditional Chinese medicine. All the CsANN proteins have four typical ANN domains, except CsANN2 and CsANN8, which lacked one and two ANN domains, respectively (Figure 3C). It is well known that a highly conserved sequence (G/KXGT-38-D/E) for binding sites of type II Ca^{2+} is present in each ANN domain in vertebrates [10]. However, the type II Ca^{2+} binding sites were absent in the repeats II and III in plant ANNs [9]. Our results also showed that repeats II and III of CsANNs did not contain the type II Ca^{2+} binding sites, which was in accordance with other plant ANNs [9]. In addition, repeat I was absent in CsANN2 and CsANN8,

 doi:10.20944/preprints202505.1673.v1

and repeat IV was absent in CsANN8 (Figure 1B). Furthermore, although four repeats were all present in the other seven CsANNs, the type II Ca^{2+} binding sites were less conserved, with two or three substitutions in repeat IV of CsANNs. Actually, the type II Ca^{2+} binding sites were only highly conserved in repeat I of CsANN1, 5, 7, and 9 (Figure 1B). Those absences of type II Ca^{2+} binding sites or the entire repeats might result in different protein conformations and largely weaken the ability of the CsANN proteins to bind to phospholipids of cell membranes in a Ca^{2+}-dependent manner, further influencing their capacities involved in plant growth and development regulation [10,11].

Another motif present in repeat I was the ILAHR sequence (Figure 1B). It was demonstrated that this sequence, especially the conserved His40 residue, played an essential role in peroxidase activity [37,38]. For example, *Arabidopsis* AnnAt1 has shown the His-residue-dependent peroxidase activity *in vitro* [16]. An AnnBr1-contained complex protein purified from *B. rapa* floral buds had peroxidase activity [39]. A maize ANN preparation also demonstrated peroxidase activity that appeared independent of heme association [37]. It is believed that the peroxidase activity of ANNs could protect the membrane from peroxidation and then subsequently improve the abiotic tolerance in plants, such as drought tolerance, etc [40,41]. As plants such as *C. saxicola* in karst regions experienced the harsh environmental conditions, the CsANNs (CsANN1, 5, 9), which present the ILAHR sequences, might contribute calcareous and drought tolerance abilities to *C. Saxicola* plants partly by the peroxidase activities.

The IRI sequence in repeat III of ANNs was highly conserved in CsANN1 and 9, and with one or two substitutions in other CsANNs except CsANN2 (Figure 1B). The IRI present in ANNs were demonstrated to bind filamentous actin (F-actin) but not globular actin in a Ca^{2+}-dependent manner, indicating these ANNs might be involved in exocytosis regulation [42]. Moreover, several ANNs of maize, cotton, and tomato were proved to hydrolyze ATP and GTP, and the nucleotide hydrolyzation abilities were attributed to the Walker A motif (GXXXXGKT/S) and the GTP binding domain (GXXG) which were retained in repeat IV of ANNs [11]. CsANN1, 5, and 9 contain a modified Walker A motif with one or two substitutions and the conserved GXXG sequence in the repeat IV, indicating their potential abilities to bind and hydrolysis GTP/ATP [45]. Interestingly, similar to *A. thaliana*, cotton, maize, and poplar, these nucleotide binding domains were partly overlapped with the Ca^{2+} binding site in repeat IV, indicating the two different binding properties were contradictory to each other and thus controlled the spatiotemporal functions of ANNs [13,18,19,46].

The phylogenetic analysis showed that CsANNs were distributed in three subfamilies, and clustered with ANNs from the dicotyledonous plants, especially the ANNs in the same genus (*C. tomentella* and *C. yanhusuo*) (Figure 2). Similar to other plant ANNs, the closely related CsANNs tend to exhibit similar structural features [22,39,47,48]. As shown in Figure 3B, motifs 1–4 are common to all CsANN members, indicating that it's crucial for CsANNs. Nevertheless, the members of subfamily II lacked motif 5, and those of subfamily III had significant differences in exon-intron structure, which may be related to functional differentiation. It is worth noting that *CsANN1* had more exons and longer introns, implying that the gene plays a more crucial role in function, expression regulation, and evolution [49–52].

3.2. CsANNs were Involved in the Biosynthesis of DHCA

It was interesting that the expression profiles of *CsANN1* and *CsANN9* in variable tissues and Ca^{2+}-treated roots of *C. saxicola* were similar to the accumulation profiles of DHCA in these treated or untreated organs, the fact of which might be an indicative of the involvement of *CsANN1/9* in DHCA biosynthesis (Figure 7, 8). In fact, transient overexpression of *CsANN*s in *C. saxicola* leaves demonstrated that higher expression of *CsANN1* could really result in the higher accumulation of BIAs, including palmatine, cheilanthifoline, dehydrocheilanthifoline, and cavidine, compared to that of EV (Figure 9C, D). Especially, compared to EV, the contents of DHCA and cheilanthifoline, a crucial upstream precursor compound of DHCA, were significantly elevated in *CsANN1*-overexpressed *C. saxicola* leaves, indicating that CsANN1 might positively regulate the expression of the genes or proteins involved in the biosynthesis pathway of cheilanthifoline and DHCA (Figure

 doi:10.20944/preprints202505.1673.v1

9D). Further analysis of candidates participated in the biosynthesis pathway of DHCA showed that the expression level of *CsBBEL9* transcripts was significantly upregulated in *CsANN1*-overexpressed *C. saxicola* leaves compared to that of EV (Figure 9B). As a result, we speculated that CsANN1 might bind directly to the DNA sequence of *CsBBEL9* in the nucleus, similar to trans-acting factors, to regulate the expression of *CsBBEL9*, and thus induce the accumulation of DHCA and its precursors. Subcellular localization analyses of CsANN1 and CsANN9 suggested a more likely presence in the cytoplasm. However, studies have shown that some *ANN*s could be introduced into the nucleus through unknown mechanisms, especially under stress conditions [9,12,47,48]. One possible assistance might be supported by the conformational changes of ANN proteins induced by N-terminal tyrosine phosphorylation, allowing the proteins to enter the nucleus [47–52]. However, more biochemical and structural evidence should be provided to confirm the subcellular localizations of *ANN*s, including *CsANN*s, during physiological processes.

Another factor influencing the accumulation of DHCA by CsANN1 might occur during the translational level. A number of cis-acting elements, including MYB binding sites, were identified in the promoters of *CsBBEL*s, *CsCMT*s, *CsOMT*s and *CsANN*s, and the Y2H assays demonstrated that CsANNs could interact with several CsMYBs in Y2HGold yeast cells (data not shown). Therefore, CsANNs-CsMYBs modules might play crucial roles in the biosynthesis pathway of DHCA. Further studies should be conducted to unravel the precise mechanisms of the biosynthesis of DHCA at transcriptional and translational levels, which could help to elucidate the adaptations of medicinal plants in karst regions.

3.3. CsANNs Might Play an Important Role in the Adaptability of C. saxicola to Karst Environment

It was reported that the calcium content in karst soil could reach up to 37.68 g/kg at most, and the average calcium availability of these soils were as high as 50.9% [29,53]. Preventing excessive absorption of Ca^{2+} is crucial for the normal growth of karst plants. For this purpose, variable unique physiological mechanisms and responsive pathways have been evolved to maintain the balance of Ca^{2+} within plant cells: (1) fixing excess Ca^{2+} by forming calcium oxalate crystals [54,55]; (2) releasing excess Ca^{2+} through stomata on mature leaves [56,57]; (3) regulating the concentration of Ca^{2+} by storing it in the intercellular spaces and organelles, such as vacuoles, endoplasmic reticulum, mitochondria, and chloroplasts [58,59]. To date, several key factors were demonstrated to be involved in these processes. For example, the Ca^{2+}/cation antiporter superfamily, which are classified into four families, H^+/cation exchangers (CAXs); Na^+/Ca^{2+} exchanger-like proteins; cation/Ca^{2+} exchangers; and Mg^{2+}/H^+ exchangers, is critical in regulating and accumulating calcium [58,60].Physilogical and genetic evidences have demonstrated that CAXs could mainly remove excess Ca^{2+} from the cytoplasm into the vacuole to maintain calcium homeostasis and alleviating calcium-induced stresses, thus granting plants the adaptation to the high-calcium karst environment [59,60]. In addition, Ca^{2+}-ATPase (ACA) could also prompt Ca^{2+} efflux from cytosol to endoplasmic reticulum, or facilate Ca^{2+} uptake from cytosol to vacuole, in an ATP-dependent manner [56]. In our study, compared with those in CK, the expression levels of several *CsCAX*s, *CsACA*s and other Ca^{2+}-balancing genes were significantly upregulated in *C. saxicola* roots treated with high concentrations of $CaCl_2$ solution (Figure S4), indicating the involvement of these factors in the adaptation of *C. saxicola* in karst landforms. In addition, the expression levels of some *CsCAX*s were much higher than those of *CsACA*s and other Ca^{2+}-balancing genes (Figure S4). This meant that the shaping of the efflux element of Ca^{2+} signatures in *C. saxicola* was mainly contributed to the expression of CsCAXs other than CsACAs, which was consistent with the fact that CAXs has lower energy consumption than ACAs and mainly act on the vacuole membrane and are more conducive to the secretion and long-term storage of Ca^{2+} [56,61]. Interestingly, significant correlations between CsANNs and Ca^{2+}-balancing genes have been identified (Figure S5), indicating the complicated adaptation styles of *C. saxicola* in calcium-rich karst ecosystems.

Except for the involvement in the adaptation of high-calcium environment, ANNs could also response to other stresses to help regulate plants' growth and development, at least partly attributing

 doi:10.20944/preprints202505.1673.v1

to the diversity of their cis-acting elements in promoters [9,18,22,25,37,48]. Multiple cis-acting elements were also identified in the promoters of *CsANN* genes (Figure 6), indicating the role of CsANNs in the adaptation of *C. saxicola* to the complex ecological environment in karst areas. For example, the ABRE elements binding sites, which could respond to ABA signals and balance cellular osmotic pressure, present in the promoters of *CsANN1*, *3*, *4*, and *9* [62,63]. All *CsANN*s possess the cis-elements of MYB transcription factors, which indicated their involvements in drought resistance by regulating ion homeostasis and reducing water loss [64,65]. In addition, ARE elements, which could activate antioxidant enzymes (such as superoxide dismutase and catalase) by binding to the nuclear factor-erythroid 2-related factor 2 or basic (region-leucine) zipper transcription factors, and thus reduce the damage caused by reactive oxygen species produced by adverse environmental factors to the membrane lipids of plants, existed in all *CsANN*s except *CsANN7* [62,66–68]. Furthermore, the *CsANNs'* promoters also contain a variety of hormone-responsive elements, such as CGTCA-motif (cis-acting regulatory element involved in the MeJA reaction), TGACG-motif (methyl jasmonate response), P-box (gibberellin response), and TGA-element (auxin response) (Table S2), all of which are conducive to alleviating stresses to the growth, development and differentiation of plants caused by arid, infertile and heavy metal pollutions [69–72]. Based on these, we speculated that CsANNs may alter the concentration of free Ca^{2+} in the cytoplasm by interacting with multiple signaling pathway genes. As Ca^{2+} is a second messenger in plants, the characteristic changes of $[Ca^{2+}]_{cyt}$ in different environments are recognized and decoded as regulatory responses in DNA, RNA, protein, or metabolic levels to help *C. saxicola* adapt in harsh karst environments.

4. Materials and Methods

4.1. Plant Materials and Treatments

C. saxicola seeds were germinated and grown in pots containing a matrix with a 3:1 mixture ratio of peat soil and vermiculite in the greenhouse (23 ℃, 16 h light, a photo flux density of 120 μmol m^{-2} s^{-1}). For the exogenous $CaCl_2$ treatment experiments, the one-month-old *C. saxicola* plants were treated with the equal volume of $CaCl_2$ at 4 mmol/L, 30 mmol/L, 100 mmol/L, 200 mmol/L, 300 mmol/L, and 400 mmol/L, respectively, for 25 d. The same batch of plants treated with the equal volume of water were set as the control (CK). The organs were then cleaned, physically isolated, and immediately frozen or dried for further research.

4.2. Genome-Wide Identification of the CsANN Genes

Firstly, the Hidden Markov Model (HMM) with the canonical *ANN* domain (Pfam00191) was used to search against the *C. saxicola* genome dataset ($P < 0.001$), which was assembled by ourselves, to identify *CsANN* genes [73]. Secondly, all eight *AtANN*s downloaded from The Arabidopsis Information Resource (TAIR) database were used as queries to retrieve *CsANN*s by BLAST in TBtools v2.096 [31]. Lastly, putative *CsANN*s were further confirmed using the InterPro and SMART databases [74]. The above non-redundant sequences were considered as *CsANN* candidates. The protein physicochemical properties of CsANNs were analyzed using the online website ExPASy [75]. Subcellular localizations of CsANNs were predicted using the online websites Wolf-psort, Cell-PLoc 2.0, CELLO, PSORT2, and Euk-mPLoc 2.0 [76–78].

4.3. Phylogenetic Relationship, Conserved Motif, and Gene Structure Analysis

The multiply alignment of the CsANNs was performed by the TBtools v2.096 [31]. The results were then visualized using the Jalview 9.0.5 [79]. The ANN protein sequences of *A. thaliana*, *B. oleracea*, *B. rapa*, *C. saxicola*, *C. tomentella*, *C. yanhusuo*, *H. vulgare*, *O. sativa*, and *P. tremula* were aligned using MEGA 11.0 [18]. The phylogenetic tree of the ANNs was constructed using the neighbor-joining method, with the bootstrap value of 1000 and other parameters set to default parameters, and then was visualized by FigTree v1.4.4. Conserved motifs of CsANNs were identified using the MEME

 doi:10.20944/preprints202505.1673.v1

Suite 5.5.7 [80]. The intron and exon regions of *CsANN*s were analyzed using the Visualize Gene Structure program in TBtools v2.096 [31].

4.4. Chromosomal Location, Collinearity, and Gene Duplication Analysis

The chromosome location information of *CsANN* genes was extracted from the *C. saxicola* plant genome gff file using the TBtools software, and visualizations were generated [31]. TBtools was further employed to conduct and visualize the collinearity analysis of the *CsANN*s. Additionally, the collinearity analysis of *A. thaliana*, *C. tomentella*, *H. vulgare*, *O. sativa*, and *P. tremula* with *C. saxicola* was performed using TBtools [31].

4.5. Cis-Acting Elements, and Protein-Protein Interaction Analysis

The 2 kb sequences upstream of the 5′ UTR of *CsANN* genes were extracted using the TBtools software and then used for the prediction of cis-acting elements based on the PlantCARE database [32]. Protein-protein interactions were predicted using the STRING database [81]. Cytoscape V3.9 was used for visualization [82].

4.6. Measurement of the BIAs Contents

An Agilent 1260 Infinity II (Agilent Co. Ltd, NY, USA) was employed to determine the relative content of the BIAs (cavidine, (s)-cheilanthifoline, dehydrocheilanthifoline, DHCA, and palmatine). Initially, 200.0 mg of dried *C. Saxicola* samples were dissolved in 10 mL of methanol and then ultrasonicated for 60 minutes. Next, the samples were centrifuged at 13,000 g for 15 min, and the supernatant was removed to a new 15-mL tube and dried using a nitrogen pressure reduction method at room temperature. Thereafter, the sample was dissolved by 1 ml of the mobile phase (acetonitrile: 0.01% K_2HPO_4 aqueous solution = 21:79 (v/v)) and filtered through a 0.22-μm filter prior to analysis. The Agilent XDBC 18 chromatographic column (150 mm × 4.6 mm, 5 μm) was used to elute the BIAs in samples under 347 nm of detection wavelength at 30 °C. The volumetric flow rate of the mobile phase (acetonitrile: 0.01% of K_2HPO_4 = 21:79 (v/v)) is 1.0 mL/min.

4.7. CsANN Cloning

The RNA was extracted from leaves, stems, and roots of *C. saxicola* before and after various treatments by FastPure Universal Plant Total RNA Isolation kit (Vazyme, Nanjing, China) based on the instruction. The first-strand cDNA was synthesized according to the instruction of HiScript Ⅲ 1st Strand cDNA Synthesis Kit (Vazyme, Nanjing, China) with the extracted total RNA as templates. To clone the full-length CDSs of *CsANN*s, the gene-specific primers (Table S3) were designed and the PCR reaction procedures were as follows: pre-denaturation at 95 ℃ for 3 min; followed by 33 cycles of denaturation at 95 ℃ for 15 s, annealing at 56 ℃ (*CsANN2*, *6*) or 54 ℃ (other *CsANN*s) for 15 s, and extension at 72 ℃ for 50 s; and a final extension at 72 ℃ for 5 min. Subsequently, PCR products were ligated into the TA/Blunt-Zero Cloning Kit vector (Vazyme, Nanjing, China) and then transformed into DH5α competent cells for incubation on LB solid medium plus 100 μg mL^{-1} kanamycin overnight. Colony PCR with the same procedure above were conducted to verify the putative positive transformants. The final CDSs of CsANNs were ascertained by Sanger sequencing.

4.8. qRT-PCR Analysis

The qRT-PCR was performed using ChamQ Universal SYBR qPCR Master Mix (Vazyme, Nanjing, China) with three technical replicates. The relative expression levels of specific genes were calculated using the 2 delta delta Ct method ($2^{-\Delta\Delta Dt}$ method), with *glyceraldehyde-3-phosphate dehydrogenase 8* (*CsGAPDH8*) used as the internal control [82–85]. The qRT-PCR primers were listed in Table S3.

 doi:10.20944/preprints202505.1673.v1

4.9. Yeast Two-Hybrid Assay

The full-length CDS of CsANNs were amplified and cloned into the destination vectors pGADT7 (pAD) and pGBKT7 (pBD), respectively. The primers used were listed in Table S3. Transactivation analysis assays were carried out in the yeast strain Y2HGold using the Yeastmaker Yeast Transformation System 2 (Clontech, Tokyo, Japan). For Y2H assays, CsANN-pAD and CsANN-pBD were transformed into Y187 and Y2HGold yeast cells, respectively. Yeast mating was conducted and the putative cotransformants were screened on SD/-Trp/-Leu (DDO) selective solid medium and then verified by PCR. SD/-Ade/-Trp/-Leu (TDO)+X+A and SD/-His/-Ade/-Trp/-Leu (QDO)+X+A were further adopted to verify the protein-protein interactions.

4.10. Transient Overexpression of CsANN1 and CsANN9 in C. saxicola Leaves

The full-length CDS of *CsANN1* and *CsANN9* were amplified and cloned into the pCAMBIA1301 vector, respectively. The primers used were listed in Table S3. The resulting plasmids were introduced into *Agrobacterium tumefaciens* GV3101. After propagation, the cells were resuspended in infiltration buffer (composed of 10 mmol/L $MgCl_2$, 10 mmol/L 2-morpholinoethanesulfonic acid, and 150 mmol/L Acetosyringone; pH 5.6) to achieve the OD_{600} of 0.8. Suspensions containing either the overexpressing constructs of the target genes *CsANN1* and *CsANN9* or the empty pCAMBIA1301 plasmid vector (serving as a control) were injected into opposite sides of the same leaf. Two days later, the injected leaves of *C. saxicola* were collected for metabolite content and gene expression analysis using HPLC and qRT-PCR, respectively [86].

5. Conclusions

In this study, we first provided a systematic analysis of the nine *CsANN* gene families in *C. saxicola*. Phylogenetic analysis of ANNs within nine species indicated that all nine CsANNs can be classified into three different subfamilies, with closely related members having similar structural characteristics. In addition, gene structures, conserved motifs, chromosomal distributions, collinearities, protein interactions, and cis-acting elements of *CsANN* genes or CsANN proteins were also analyzed. Expression pattern analysis unraveled two candidates, *CsANN1* and *CsANN9*, as the putative positive regulators involved in the biosynthesis of DHCA in *C. saxicola*. Further experiments indicated that transient overexpression of *CsANN1*, but not *CsANN9*, could increase the content of DHCA in *C. saxicola* leaves. This study provides a theoretical basis for understanding the biological functions of the CsANNs in secondary metabolites and adaptation to adverse stresses of *C. saxicola*.

Supplementary Materials: The following supporting information can be downloaded at Preprints.org, Figure S1: The biosynthetic pathway of BIAs. (Each color represents a branch of different secondary metabolites synthesized by scoulerine, green: the biosynthetic pathway of palmatine synthesized by scoulerine; blue: the predicted biosynthetic pathway of DHCA synthesized from scoulerine; yellow: the biosynthetic pathway of sanguinarine synthesized from scoulerine; purple: the biosynthetic pathway of codeine and morphine synthesized from scoulerine. TYDC: L-tyrosine decarboxylase; TAT: tyrosine aminotransferase; TYR: tyrosine 3-monooxygenase; HPPDC: 4-hydroxyphenylpyruvate dioxygenase; NCS: norcoclaurine synthase; 6OMT: norcoclaurine 6 O-methyltransferase; CNMT: coclaurine N-methyltransferase; NMCH: N-methylcoclaurine 3'-hydroxylase; 4'OMT: 3'-hydroxy-N-methylcoclaurine 4'-O-methyltransferase; BBE: berberine bridge enzyme; 9OMT: scoulerine 9-O-methyltransferase; BBEL: berberine bridge enzyme-like; OMT: O-methyltransferase; CMT: C-methyltransferase; CFS: cheilanthifoline synthase; SPS: stylopine synthase; TNMT: tetrahydroprotoberberine N-methyltransferase; MSH: N-methylstylopine 14-hydroxylase; P6H: protopine 6-hydroxylase; DBOX: dihydrobenzophenanthridine oxidase; REPI: reticuline epimerase; SalSyn, salutaridine synthase); Figure S2: Correlation analysis of *CsOMT*s, *CsCMT*s, and *CsBBEL*s with *CsANN*s; Figure S3: The transient overexpression and functional analysis of and CsANN9 (Expression profiles of *CsANN9* and other genes in *C. saxicola* leaves infiltrated with *CsANN9*-pCAMBIA1301 or *EV* (A), Changes in BIA contents in *C. saxicola* leaves infiltrated with CsANN9-pCAMBIA1301 or *EV* (B), Statistic analysis of BIA contents in *C. saxicola*

 doi:10.20944/preprints202505.1673.v1

leaves infiltrated with CsANN9-pCAMBIA1301 or *EV*(C)); Figure S4: Expression of the genes involved in Ca^{2+} sensor and signal-relay pathways in *C. saxicola* under different concentrations of $CaCl_2$ solution (CIPK, CBL-interacting protein; CAM, calmodulin; CML, calmodulin-like gene; GLR, glutamate-like receptors; CDPK, calcium-dependent protein kinase; CBL, calcineurin B-like protein; CAX, vacuolar Ca^{2+} exchanger; ACA, Ca^{2+}-ATPase; CNGC, cyclic nucleotide-gated channel); Figure S5: Correlation analysis of the genes involved in Ca^{2+} sensor and signal-relay pathways with *CsANN*s; Table S1: Identification and physicochemical analysis of CsANNs; Table S2: The cis-acting elements identified in *CsANN* promoters; Table S3: Primers used in this study; Table S4. The accession numbers of genes involved in the study.

Author Contributions: Conceptualization, L.H. and X.O.; methodology, L.H. and Z.W.; data curation, L.K. and Y.L.; writing—original draft preparation, H.L. and M.L.; writing—review and editing, H.L., J.W. and M.L.; project administration, M.Q. and Z.W.; funding acquisition, C.L. and Z.Z. All authors have read and agreed to the published version of the manuscript.

Funding: This research was funded by the Guangxi Science and Technology Base and Talent Project (Guike AD22080016); the Natural Science Foundation of Guangxi (2025GXNSFBA069023; 2025GXNSFAA069814; 2023GXNSFAA026509); the National Natural Science Foundation of China (32460105 and 32260107); Guangxi Key R&D Program (Guike AB23026092); the Central Guidance on Local Science and Technology Development Fund of Guangxi (GK ZY24212031); Guangxi Key Laboratory of Medicinal Resources Protection and Genetic Improvement (KL2022ZZ04, KL2023ZZ09 and KL2023KF04).

Data Availability Statement: All relevant data are within the manuscript and its Additional files.

Conflicts of Interest: The authors declare no conflicts of interest.

References

1. Yan, G.; Lin, Z.; Bo, C.; Jia, Y.; Jiang, B.; Qi, Y.; Jun, L. The Traditional Uses, Phytochemistry, Pharmacokinetics, Pharmacology, Toxicity, and Applications of *Corydalis Saxicola* Bunting: A Review. *Front. Pharmacol.* **2022**, *13*, 822792. [CrossRef] [PubMed]
2. Xu, L.; Chao, T.; Hua, Z.; Jin, W.; Fang, W.; Yi, Y.M.; Xi, L.; Hong, Z.; Chun, Y.; Bang, C.; et al. Investigation of the Hepato-protective Effect of *Corydalis Saxicola* Bunting on Carbon Tetrachloride-Induced Liver Fibrosis in Rats by ^{1}H-NMR-Based Metabonomics and Network Pharmacology Approaches. *J. Pharm. Biomed. Anal.* **2018**, *159*, 252–261. [CrossRef] [PubMed]
3. Feng, Q.; Yao, C.; Fan, W.; Shao, T.; Yi, F. *Corydalis Saxicola* Bunting: A Review of Its Traditional Uses, Phytochemistry, Pharmacology, and Clinical Applications. *Int. J. Mol. Sci.* **2023**, *24*, 1626. [CrossRef] [PubMed]
4. Fan, Z.; Yang, X.; Zhen, L.; Xiao, W.; Dan, H.; Sui, Z.; Min, L.; De, Y.; Dong, W.; Yi, W. Anti-Hepatitis B Virus Effects of Dehydrocheilanthifoline from *Corydalis Saxicola*. *Am. J. Chin. Med.* **2013**, *41*, 119–130. [CrossRef] [PubMed]
5. Wang, T.; Sun, N.L.; Zhang, W.D.; Li, H.L.; Lu, G.C.; Yuan, B.J.; Jiang, H.; She, J.H.; Zhang, C. Protective Effects of Dehy-drocavidine on Carbon Tetrachloride-Induced Acute Hepatotoxicity in Rats. *J. Ethnopharmacol.* **2008**, *117*, 300–308. [CrossRef] [PubMed]
6. Li, C.; Liu, H.; Qin, M.; Tan, Y.J.; Ou, X.L.; Chen, X.Y.; Wei, Y.; Zhang, Z.J.; Lei, M. RNA Editing Events and Expression Profiles of Mitochondrial Protein-Coding Genes in the Endemic and Endangered Medicinal Plant, *Corydalis Saxicola*. *Front. Plant Sci.* **2024**, *15*, 1332460. [CrossRef] [PubMed]
7. Liu, C.X.; Duan, Y.; Xie, H.T.; Tian, J. Challenges in Research and Development of Traditional Chinese Medicines. Institute of Pharmaceutical Research. Nanjing, China, 2007: 7102–8.
8. Hui, L.; Wei, Z.; Chuan, Z.; Ting, H.; Run, L.; Jiang, H.; Hai, C. Comparative Analysis of the Chemical Profile of Wild and Cultivated Populations of *Corydalis Saxicola* by High-Performance Liquid Chromatography. *Phytochem. Anal.* **2007**, *18*, 393–400. [CrossRef] [PubMed]
9. Xiao, W.; Yan, W.; Yu, B.; Yan, R.; Xiao, X.; Fu, Z.; Hai, D. A Critical Review on Plant Annexin: Structure, Function, and Mechanism. *Plant Physiol. Biochem.* **2022**, *190*, 81–89. [CrossRef] [PubMed]

 doi:10.20944/preprints202505.1673.v1

10. Volker, G.; Carl, C.; Stephen, M. Annexins: Linking Ca; Signalling to Membrane Dynamics. *Nat. Rev. Mol. Cell Biol.* **2005**, *6*, 449–461. [CrossRef] [PubMed]
11. C, M.J.; Anuphon, L.; Neil, M.; Alex, W.; Colin, B.; H, B.N.; M, D.J. Annexins: Multifunctional Components of Growth and Adaptation. *J. Exp. Bot.* **2008**, *59*, 533–544. [CrosRef] [PubMed]
12. Joanna, P.; Aneta, K.; Ruud, D.; Marcin, G.; Michael, K.; Jean, L.; Slawomir, P.; René, B. A Putative Consensus Sequence for the Nucleotide-Binding Site of Annexin A6. *Biochemistry.* **2003**, *42*, 9137–9146. [PubMed]
13. Michaela, T.; Hendrik, R.; Miroslav, O.; Nicola, M.; Miroslava, H.; Petr, D.; Jozef, Š.; Olga, Š. Advanced Microscopy Reveals Complex Developmental and Subcellular Localization Patterns of ANNEXIN 1 in Arabidopsis. *Front. Plant Sci.* **2020**, *11*, 1153. [CrossRef] [PubMed]
14. Volker, G.; E, M.S. Annexins: From Structure to Function. *Physiol. Rev.* **2002**, *82*, 331–371. [PubMed]
15. A, H.; J, P.; A, D.; R, S.; R, H. Annexin 24 from *Capsicum Annuum* X-Ray Structure and Biochemical Characterization. *J. Biol. Chem.* **2000**, *275*, 8072–8082. [PubMed]
16. Dorota, P.; Greg, C.; Grazyna, G.; Janusz, D.; Krzysztof, F.; Araceli, C.; Bartlomiej, F.; Stanley, R.; Jacek, H. The Role of Annexin 1 in Drought Stress in Arabidopsis. *Plant Physiol.* **2009**, *150*, 1394–1410. [CrossRef] [PubMed]
17. B, C.G.; A, S.; J, E.D.; J, R.S. Differential Expression of Members of the Annexin Multigene Family in Arabidopsis. *Plant Physiol.* **2001**, *126*, 1072–1084. [CrossRef] [PubMed]
18. Hui, W.; Ali, M.; Guo, L.; Yi, L.; Shi, L.; Chun, Y.; Yan, C.; Fei, Z.; Jian, Z. Genome-Wide Characterization and Abiotic Stresses Expression Analysis of Annexin Family Genes in Poplar. *Int. J. Mol. Sci.* **2022**, *23*, 515. [CrossRef] [PubMed]
19. Mei, Z.; Xiong, Y.; Qian, Z.; Ming, Z.; En, Z.; Yi, T.; Xue, Z.; Ji, S.; Yan, W. Induction of Annexin by Heavy Metals and Jasmonic Acid in *Zea Mays*. *Funct. Integr. Genomics* **2013**, *13*, 241–251. [CrossRef] [PubMed]
20. Yadav, D.; Ahmed, I.; Kirti, P.B. Genome-Wide Identification and Expression Profiling of Annexins in *Brassica Rapa* and Their Phylogenetic Sequence Comparison with *B. Juncea* and *A. Thaliana* Annexins. *Plant Gene* **2015**, *4*, 109–124. [CrossRef]
21. Feng, S.; Jia, Y.; Liang, X.; Xiao, S.; Ji, W.; Yan, W.; Yi, M.; Yue, Z.; Li, L. Characterization of *Annexin* Gene Family and Func-tional Analysis of *RsANN1a* Involved in Heat Tolerance in Radish (*Raphanus Sativus* L.). *Physiol. Mol. Biol. Plants* **2021**, *27*, 2027–2041. [CrossRef] [PubMed]
22. Kumar, J.S.; B, C.G.; T, A.B.; J, R.S.; B, K.P. Identification and Characterization of Annexin Gene Family in Rice. *Plant Cell Rep.* **2012**, *31*, 813–825. [CrossRef] [PubMed]
23. Feng, Y.M.; Wei, X.K.; Liao, W.X.; Huang, L.H.; Zhang, H.; Liang, S.C.; Peng, H. Molecular Analysis of the Annexin Gene Family in Soybean. *Biol. plant.* **2013**, *57*, 655–662. [CrossRef]
24. Hee, Y.; Pat, H.; Venkatesan, S. Analysis of the Female Gametophyte Transcriptome of Arabidopsis by Comparative Expression Profiling. *Plant Physiol.* **2005**, *139*, 1853–1869. [PubMed]
25. Cantero, A.; Barthakur, S.; Bushart, T.; Chou, S.; Morgan, R.; Fernandez, M.; Clark, G.; Roux, S. Expression Profiling of the Arabidopsis Annexin Gene Family during Germination, de-etiolation and Abiotic Stress. *Plant Physiol. Biochem. (Issy-les-Moulineaux, Fr.)* **2006**, *44*, 13–24. [CrossRef] [PubMed]
26. Guy, B.; Heidi, N.; Jeppe, E.; L, N.K.; Malene, J.; G, W.K. Patatins, Kunitz Protease Inhibitors and Other Major Proteins in Tuber of Potato Cv. Kuras. *FEBS J.* **2006**, *273*, 3569–3584. [CrossRef] [PubMed]
27. D, S.; N, R.; J, D.A.; J, J. Sulfolipid Is a Potential Candidate for Annexin Binding to the Outer Surface of Chloroplast. *Biochem. Biophys. Res. Commun.* **2000**, *272*, 519–524. [CrossRef] [PubMed]
28. Patrick, G.; Kristin, K.; Anna, K.; Anja, B.; Julia, K. Towards the Proteome of *Brassica Napus* Phloem Sap. *Proteomics* **2006**, *6*, 896–909. [CrossRef] [PubMed]
29. Tang, J.; Tang, X.; Qin, Y.; He, Q.; Yi, Y.; Ji, Z. Karst Rocky Desertification Progress: Soil Calcium as a Possible Driving Force. *Sci. Total. Environ.* **2019**, *649*, 1250–1259. [CrossRef] [PubMed]
30. Zhi, L.; Li, Z.; Zhong, Y.; Zhi, R.; Feng, H.; Xin, T.; Zhi, X.; Fang, D.; Zuo, Y.; Guang, L.; et al. Genomic Mechanisms of Physiological and Morphological Adaptations of *Limestone Langurs* to Karst Habitats. *Mol. Biol. Evol.* **2020**, *37*, 952–968. [CrossRef] [PubMed]

 doi:10.20944/preprints202505.1673.v1

31. Cheng, C.; Hao, C.; Yi, Z.; Hannah, T.; Margaret, F.; Ye, H.; Rui, X. TBtools: An Integrative Toolkit Developed for Interactive Analyses of Big Biological Data. *Mol. Plant* **2020**, *13*, 1194–1202. [CrossRef] [PubMed]
32. Magali, L.; Patrice, D.; Gert, T.; Kathleen, M.; Yves, M.; Peer, V.; Pierre, R.; Stephane, R. PlantCARE, a Database of Plant Cis-Acting Regulatory Elements and a Portal to Tools for in Silico Analysis of Promoter Sequences. *Nucleic Acids Res.* **2002**, *30*, 325–327. [PubMed]
33. Xu, Z.; Li, Z.; Ren, F.; Gao, R.; Wang, Z.; Zhang, J.; Zhao, T.; Ma, X.; Pu, X.; Xin, T.; et al. The Genome of Corydalis Reveals the Evolution of Benzylisoquinoline Alkaloid Biosynthesis in Ranunculales. *Plant J.* **2022**, *111*, 217–230. [PubMed]
34. Ferré, S.; Casadó, V.; Devi, L.A.; Filizola, M.; Jockers, R.; Lohse, M.J.; Milligan, G.; Pin, P.; Guitart, X. G Protein–Coupled Re-ceptor Oligomerization Revisited: Functional and Pharmacological Perspectives. *Pharmacol. Rev.* **2014**, *66*, 413–434. [CrossRef] [PubMed]
35. Delaux, M.; Séjalon, N.; Bécard, G.; Ané, M. Evolution of the Plant-Microbe Symbiotic "Toolkit". *Trends Plant Sci* **2013**, *18*, 298–304. [CrossRef] [PubMed]
36. Jami, K.; Clark, B.; Ayele, T.; Ashe, P.; Kirti, B. Genome-Wide Comparative Analysis of Annexin Superfamily in Plants. *PLoS One* **2012**, *7*, e47801. [CrossRef] [PubMed]
37. C, M.J.; M, C.K.; Anuphon, L.; M, D.J. Heme-Independent Soluble and Membrane-Associated Peroxidase Activity of a *Zea Mays* Annexin Preparation. *Plant signaling behave.* **2009**, *4*, 428–430. [CrossRef] [PubMed]
38. M, G.K.; Dorota, K.; Jacek, H.; Rene, B.; Slawomir, P. Peroxidase Activity of Annexin 1 from *Arabidopsis Thaliana*. *Biochem. Biophys. Res. Commun.* **2005**, *336*, 868–875. [CrossRef] [PubMed]
39. Xin, H.; Li, L.; Sai, X.; Min, Y.; Pan, X.; Wei, L.; Yu, K.; Lu, H.; Mei, W.; Lun, Q.; et al. Comprehensive Analyses of the Annexin (*ANN*) Gene Family in *Brassica Rapa*, *Brassica Oleracea* and *Brassica Napus* Reveals Their Roles in Stress Response. *Sci. Rep.* **2020**, *10*, 4295. [CrossRef] [PubMed]
40. Raina, I.; Javeria, E.; Sheng, G.; Teng, L.; Muhammad, I.; Zhi, Y.; Taotao, W. Overexpression of Annexin Gene *AnnSp2*, Enhances Drought and Salt Tolerance through Modulation of ABA Synthesis and Scavenging ROS in Tomato. *Sci. Rep.* **2017**, *7*, 12087. [CrossRef] [PubMed]
41. Feng, Z.; Shufen, L.; Shu, Y.; Like, W.; Wang, G. Retraction Note to: Overexpression of a Cotton Annexin Gene, *GhAnn1*, Enhances Drought and Salt Stress Tolerance in Transgenic Cotton. *Plant Mol. Biol.* **2018**, *98*, 185. [CrossRef] [PubMed]
42. Hoshino, D.; Hayashi, A.; Temi, Y.; Kan, N.; Tsuchiya, T. Biochemical and Immunohistochemical Characterization of *Mimosa* Annexin. *Planta* **2004**, *219*, 867–875. [CrossRef] [PubMed]
43. Forero, C.; Wasserman, M. Isolation and Identification of Actin-Binding Proteins in Plasmodium Falciparum by Affinity Chromatography. *Mem. Inst. Oswaldo Cruz* **2000**, *95*, 329–337. [CrossRef] [PubMed]
44. Calvert, C.M.; Gant, S.J.; Bowles, D.J. Tomato Annexins P34 and P35 Bind to F-Actin and Display Nucleotide Phosphodiesterase Activity inhibited by Phospholipid Binding. *Plant cell* **1996**, *8*, 333-342. [PubMed]
45. Nien, H.; Mohd, Y.A.; An, W.; Asiah, O.; K, R.A.; Andreas, H. The Crystal Structure of Calcium-Bound Annexin Gh1 from *Gossypium Hirsutum* and Its Implications for Membrane Binding Mechanisms of Plant Annexins. *J. Biol. Chem.* **2008**, *283*, 18314–18322. [CrossRef] [PubMed]
46. Feng, Z.; Xuan, J.; Like, W.; Shu, L.; Shuang, W.; Chao, C.; Tian, Z.; Wang, G. A Cotton Annexin Affects Fiber Elongation and Secondary Cell Wall Biosynthesis Associated with Ca^{2+} Influx, ROS Homeostasis, and Actin Filament Reorganization. *Plant Physiol.* **2016**, *171*, 1750–1770. [CrossRef] [PubMed]
47. Liu, X.; Zhang, M.; Zhao, X.; Shen, M.; Feng, R.; Wei, Q. The Evolution, Variation and Expression Patterns of the Annexin Gene Family in the Maize Pan-Genome. *Sci. Rep.* **2025**, *15*, 5711. [CrossRef] [PubMed]
48. Chen, L.; Chen, K.; Xi, X.; Du, X.; Zou, X.; Ma, Y.; Song, Y.; Luo, C.; Wei, S. The Evolution, Expression Patterns, and Domes-tication Selection Analysis of the Annexin Gene Family in the Barley Pan-Genome. *Int. J. Mol. Sci.* **2024**, *25*. [CrossRef] [PubMed]
49. Gil, A. The Alternative Genome. *Sci. Am.* **2005**, *292*, 40–47. [PubMed]
50. Barmak, M.; Christopher, L. A Genomic View of Alternative Splicing. *Nat. Genet.* **2002**, *30*, 13–19. [PubMed]
51. Jeffares, D.C.; Penkett, J.; Bähler, J. Rapidly Regulated Genes Are Intron Poor. *Trends Genet.* **2008**, *24*, 375–378. [CrossRef] [PubMed]

 doi:10.20944/preprints202505.1673.v1

52. William, R.S.; Walter, G. The Evolution of Spliceosomal Introns: Patterns, Puzzles and Progress. *Nat. Rev. Genet.* **2006**, *7*, 211–221. [CrossRef] [PubMed]
53. Maranhão, C.; Pereira, G.; Collier, L.S.; Anjos, L.H.C.; Azevedo, A.C.; Souza, R. Pedogenesis in a Karst Environment in the Cerrado Biome, Northern Brazil. *Geoderma* **2020**, *365*, 114169. [CrossRef]
54. Volk, G.M.; Lynch, V.J.; Kostman, T.A.; Goss, L.J.; Franceschi, V.R. The Role of Druse and Raphide Calcium Oxalate Crystals in Tissue Calcium Regulation in *Pistia stratiotes* Leaves. *Plant Biol. (Berlin, Ger.)* **2002**, *4*, 34–45. [CrossRef]
55. Ilarslan, H. Calcium Oxalate Crystals in Developing Seeds of Soybean. *Ann. Bot. (Oxford, U. K.)* **2001**, *88*, 243–57. [CrossRef]
56. Wei, X.; Deng, X.; Xiang, W. Calcium content and high calcium adaptation of plants in karst areas of southwestern Hunan, China. *Biogeosciences* **2018**, *15*, 2991–3002. [CrossRef]
57. Musetti, R.; Favali, M. Cytochemical localization of calcium and X-ray microanalysis of *Catharanthus roseus* L. infected with phytoplasmas. *Micron* 2003, 34, 387–393 [CrossRef] [PubMed]
58. Hanger, B.C. The movement of calcium in plants. *Commun. Soil Sci. Plant Anal.* **1979**, *10*, 171–193. [CrossRef] [PubMed]
59. Poovaiah, B.W.; Reddy, A.S.N.; Leopold, A.C. Calcium messenger system in plants. *Crit. Rev. Plant Sci.* **1987**, *6*, 47–103. [PubMed]
60. Zhou, Y.; Fan, W.; Zhang, H. *Marsdenia tenacissima* genome reveals calcium adaptation and tenacissoside biosynthesis. *Plant J.* **2022**, *113*, 1146–1159. [PubMed]
61. Huang, H.; Yang, Y.; Li, J. Effects of Rocky Desertification Stress on Oat (*Avena sativa* L.) Seed Germination and Seedling Growth in the Karst Areas of Southwest China. *Plants* **2024**, *13*, 3260–3260. [CrossRef] [PubMed]
62. Ya, L.; Xuan, X.; Lu, G.; Jia, Z.; Chao, G.; Zhi, W.; Hong, L.; Xing, L.; Xiao, Y.; Na, Z.; et al. CsbZIP50 Binds to the G-Box/ABRE Motif in *CsRD29A* Promoter to Enhance Drought Tolerance in Cucumber. *Environ. Exp. Bot.* **2022**, *199*, 104884. [CrossRef]
63. Zheng, J.; Wen, D.; Tang, C.; Lai, S.; Yan, Y.; Du, C.; Zhang, Z. The Transcriptional Regulation of Arabidopsis *ECT8* by ABA-Responsive Element Binding Transcription Factors in Response to ABA and Abiotic Stresses. *Physiol. Mol. Biol. Plants* **2025**, *31*, 1–13. [CrossRef] [PubMed]
64. Wang, X.; Wei, H.; Wang, K.; Tang, X.; Li, S.; Zhang, N.; Si, H. MYB Transcription Factors: Acting as Molecular Switches to Regulate Different Signaling Pathways to Modulate Plant Responses to Drought Stress. *Ind. Crops Prod.* **2025**, *226*, 120676. [CrossRef]
65. Liu, Z.; Li, J.; Li, S.; Song, Q.; Miao, M.; Fan, T.; Tang, X. The 1R-MYB Transcription Factor SlMYB1L Modulates Drought Tol-erance via an ABA-Dependent Pathway in Tomato. *Plant Physiol. Biochem.* **2025**, *222*, 109721. [CrossRef] [PubMed]
66. Li, Y.; Li, Y.; Lu, H. The bZIP transcription factor ATF1 regulates blue light and oxidative stress responses in *Trichoderma guizhouense*. *mLife* **2023**, *2*, 365–77. [CrossRef] [PubMed]
67. Wang, X.; Wu, F.; Liu, L. The bZIP transcription factor PfZipA regulates secondary metabolism and oxidative stress response in the plant endophytic fungus *Pestalotiopsis fici*. *Fungal Genet. Biol.* **2015**, *81*, 221–228. [CrossRef] [PubMed]
68. Wang, X.; Zha, W.; Liang, L.; Faso, O.E.; Wu, L.; Wang, S. The bZIP Transcription Factor AflRsmA Regulates Aflatoxin B_1 Biosynthesis, Oxidative Stress Response and Sclerotium Formation in *Aspergillus flavus*. *Toxins* **2020**, *12*, 271. [CrossRef] [PubMed]
69. M, G.; N, F.; E, G.; E, M.; G, P.M. The *ACA4* Gene of Arabidopsis Encodes a Vacuolar Membrane Calcium Pump That Improves Salt Tolerance in Yeast. *Plant Physiol.* **2000**, *124*, 1814–1827. [CrossRef] [PubMed]
70. Liu, L.; Yahaya, S.; Li, J.; Wu, F. Enigmatic Role of Auxin Response Factors in Plant Growth and Stress Tolerance. *Front. Plant Sci.* **2024**, *15*, 1398818. [CrossRef] [PubMed]
71. Yuan, Y.; Stéphanie, S.; Aurore, C. A downstream mediator in the growth repression limb of the jasmonate pathway. *Plant Cell* **2007**, *19*, 2470–2483. [CrossRef] [PubMed]
72. Kazuko, Y.S.; Kazuo, S. Organization of Cis-Acting Regulatory Elements in Osmotic- and Cold-Stress-Responsive Promoters. *Trends Plant. Sci.* **2005**, *10*, 88–94. [PubMed]

 doi:10.20944/preprints202505.1673.v1

73. M, S.; C, S.; J, C.E. Gene Hunting with Hidden Markov Model Knockoffs. *Biometrika* **2019**, *106*, 1–18. [PubMed]
74. Lorna, R.; Neil, R.; Gustavo, S.; Alexandre, A.; David, H.; Gregory, D.; Granger, S.; Robert, F. Genome Properties in 2019: A New Companion Database to InterPro for the Inference of Complete Functional Attributes. *Nucleic Acids Res.* **2019**, *47*, D564–D572. [CrossRef] [PubMed]
75. Séverine, D.; Chiara, G.; Frédérique, L.; Heinz, S.; Vassilios, I.; Christine, D. Expasy, the Swiss Bioinformatics Resource Portal, as Designed by Its Users. *Nucleic Acids Res.* **2021**, *49*, W216–W227.
76. Ivica, L.; Leo, G.; J, D.N.; Tobias, D.; Joerg, S.; Richard, M.; Francesca, C.; R, C.R.; P, P.C.; Peer, B. Recent Improvements to the SMART Domain-Based Sequence Annotation Resource. *Nucleic Acids Res.* **2002**, *30*, 242–244. [PubMed]
77. Kuo, C.; Hong, S. Cell-PLoc: A Package of Web Servers for Predicting Subcellular Localization of Proteins in Various Organisms. *Nat. Protoc.* **2008**, *3*, 153–162. [CrossRef] [PubMed]
78. Kuo, C.; Hong, S. Euk-mPLoc: A Fusion Classifier for Large-Scale Eukaryotic Protein Subcellular Location Prediction by Incorporating Multiple Sites. *J. Proteome Res.* **2007**, *6*, 1728–1734. [PubMed]
79. Andrew, W.; Jim, P.; David, M.; Geoffrey, B. Jalview: Visualization and Analysis of Molecular Sequences, Alignments, and Structures. *BMC Bioinform.* **2005**, *6*, P28. [CrossRef]
80. Bailey, T.L.; Johnson, J.; Grant, C.E.; Noble, W.S. The MEME Suite. *Nucleic Acids Res.* **2015**, *43*, W39–W49. [CrossRef] [PubMed]
81. Szklarczyk, D.; Nastou, K.; Koutrouli, M.; Kirsch, R.; Mehryary, F.; Hachilif, R.; Hu, D.; Peluso, M.E.; Huang, Q.; Fang, T.; et al. The STRING Database in 2025: Protein Networks with Directionality of Regulation. *Nucleic Acids Res.* 2024. [CrossRef] [PubMed]
82. David, O.; John, M.; Jorge, B.; Alexander, P.; Barry, D. Cytoscape Automation: Empowering Workflow-Based Network Analysis. *Genome Biol.* **2019**, *20*, 185. [CrossRef] [PubMed]
83. Zhu, Y.; Niu, S.; Lin, J.; Yang, H.; Zhou, X.; Wang, S.; Liu, X.; Yang, Q.; Zhang, C.; Zhuang, Y.; et al. Genome-Wide Identification and Expression Analysis of *TCP* Transcription Factors Responding to Multiple Stresses in *Arachis Hypogaea* L. *Int. J. Mol. Sci.* **2025**, *26*, 1069. [CrossRef] [PubMed]
84. Shao, Y.; Mu, D.; Zhou, Y.; Liu, X.; Huang, X.; Wilson, I.W.; Qi, Y.; Lu, Y.; Zhu, L.; Zhang, Y.; et al. Genome-Wide Mining of CULLIN E3 Ubiquitin Ligase Genes from *Uncaria Rhynchophylla*. *Plants* **2024**, *13*, 532. [CrossRef] [PubMed]
85. Dong, X.; Lv, M.; Zeng, M.; Chen, X.; Wang, J.; Liang, X.F. Genome-Wide Identification, Characterization of the ORA (Olfactory Receptor Class A) Gene Family, and Potential Roles in Bile Acid and Pheromone Recognition in Mandarin Fish (*Siniperca Chuatsi*). *Cells* **2025**, *14*, 189. [CrossRef] [PubMed]
86. Jia, W.; Ya, W.; Xu, L.; Hui, P.; Dian, J.; Jia, W.; Can, J.; Kumar, S.S.; Jian, S.; Xin, L.; et al. An Integrated Multi-Omics Approach Reveals Polymethoxylated Flavonoid Biosynthesis in *Citrus Reticulata* cv. Chachiensis. *Nat. Commun.* **2024**, *15*, 3991. [CrossRef] [PubMed]